The Astrophysical Journal Letters, 872:L22 (7pp), 2019 February 20 https://doi.org/10.3847/2041-8213/ab0286

No Stripped Companion Material in the Nebular Spectrum of the "Two-Component" Type Ia Supernova ASASSN-18bt

M. A. Tucker[1,3], B. J. Shappee[1], and J. P. Wisniewski[2]
[1] Institute for Astronomy, University of Hawai'i, 2680 Woodlawn Drive, Honolulu, HI 96822, USA; tuckerma@hawaii.edu
[2] Homer L. Dodge Department of Physics & Astronomy, The University of Oklahoma, 440 West Brooks Street, Norman, OK 73019, USA
Received 2018 November 22; revised 2019 January 17; accepted 2019 January 29; published 2019 February 19

Abstract

We analyze a Keck I/Low Resolution Imager and Spectrograph nebular spectrum taken 268 days after *B*-band maximum of ASASSN-18bt (SN 2018oh), a Type Ia supernova observed by *K2* at the time of explosion. ASASSN-18bt exhibited a two-component rise to peak brightness, possibly the signature of an interaction between the supernova ejecta and a large ($\gtrsim$20 $R_\odot$) nearby, non-degenerate companion. We search for emission signatures of stripped material from a non-degenerate companion in the nebular spectrum and find no evidence for any unbound material. We place an upper limit of $<0.006\,M_\odot$ on the amount of stripped/ablated H-rich material that could go undetected in our spectrum, effectively ruling out all hydrogen-rich donor stars. Additionally, we place a more tentative upper limit on He I emission in the observed spectrum of $\lesssim 0.02\,M_\odot$ which also rules out helium star companions. Our deep limits rule out a non-degenerate companion as the explanation for the early-time feature in ASASSN-18bt.

Key words: supernovae: general – supernovae: individual (ASASSN-18bt/SN2018oh) – techniques: spectroscopic

1. Introduction

Although Type Ia supernova (SN Ia) have been anchors for cosmological studies, their origins remain elusive. The consensus is that they originate from a carbon/oxygen (C/O) white dwarf (WD) experiencing a thermonuclear explosion (Hoyle & Fowler 1960), although the mechanism for actually exploding the WD is still debated. The current literature on SNe Ia progenitors can be grouped into two broad categories: the single-degenerate (SD) and double-degenerate (DD) scenarios (see Maoz et al. 2014 for an in-depth review).

The DD scenario involves two WDs colliding or coalescing to produce an SN Ia. The exact merger process is unclear, with theories including gravitational wave emission from a close binary (e.g., Tutukov & Yungelson 1979; Iben & Tutukov 1984; Webbink 1984), a violent collision due to perturbations from a third (e.g., Thompson 2011; Katz et al. 2012; Shappee & Thompson 2013; Antognini et al. 2014) or fourth body (e.g., Pejcha et al. 2013), runaway accretion from the lower-mass WD onto the smaller, more massive WD (e.g., Pakmor et al. 2012), or a "double-detonation," where an initial detonation in an accreted He surface layer triggers carbon detonation in the core of the sub-Chandrasekhar mass WD (Fink et al. 2010; Kromer et al. 2010). As both stars involved in this process are intrinsically faint, finding and characterizing these systems is exceptionally difficult (e.g., Rebassa-Mansergas et al. 2019). However, some tentative progress has been made, such as bimodal emission in the nebular phase (Dong et al. 2015), constraints on nucleosynthetic yields (e.g., Shappee et al. 2017), and potential hyper-velocity remnants (Shen et al. 2018). No concrete detections of a DD system have been discovered thus far, and the majority of DD progenitor conclusions stem from ruling out SD systems.

In the SD case, the WD has a non-degenerate companion, such as a main sequence (MS), sub giant (SG), or red giant (RG) star, undergoing Roche Lobe overflow (RLOF). Mass-transfer onto the WD occurs until the WD is destabilized and explodes. There are several observational signatures expected from the SD channel of SNe Ia regardless of the explosion mechanism. X-rays are expected from the accretion onto the WD (Lanz et al. 2005), which should have observational signatures many years after explosion (e.g., Woods et al. 2018). When the ejecta strikes the companion, $\sim$0.15–0.5 $M_\odot$ of mass will be stripped/ablated from the donor star (Marietta et al. 2000; Pan et al. 2012; Boehner et al. 2017), and should be visible once the SN Ia enters the nebular phase (Mattila et al. 2005; Botyánszki et al. 2018). Additionally, the ejecta-companion interaction should create a blue signature in the rising light curve detectable within the first 1–2 days after explosion (Kasen 2010). Assuming RLOF, these signatures are dependent on both the radius of the companion and the viewing angle of the explosion, which can mask potential detections.

Modern surveys have become increasing capable of discovering nearby SNe within a day or two after explosion and probing the early light curves of SNe Ia. There are many SNe Ia that show smoothly rising light curves (e.g., Nugent et al. 2011; Cartier et al. 2017; Holmbo et al. 2018), yet some exhibit a rise to peak that does not follow a single power law (e.g., SN 2012fr, Contreras et al. 2018; SN 2013dy, Zheng et al. 2013; SN 2014J Goobar et al. 2015, Siverd et al. 2015; MUSSES1604D Jiang et al. 2017; iPTF16abc Miller et al. 2018; and SN 2017cbv Hosseinzadeh et al. 2017) with ASASSN-18bt falling into this category (Shappee et al. 2019). This deviation from a single power-law rise has been interpreted as potential ejecta-companion interaction (e.g., SN 2017cbv, Hosseinzadeh et al. 2017), especially when accompanied by a blue excess. Yet searches for other expected signatures of SD progenitor systems in SN 2017cbv return null results (Sand et al. 2018). The difference between these two types of early SNe Ia light curves can potentially be explained by the viewing angle, but it is still unclear if these deviations are truly indicative of ejecta-companion interaction, or suggestive of other physical processes intrinsic to the SN Ia explosion.

[3] DOE CSGF Fellow.

Stritzinger et al. (2018) recently uncovered two distinct SN Ia populations in observations of SNe Ia within days after explosion that had definitive red and blue populations before converging to a single relation. Furthermore, the presence of a blue excess at early times is correlated with photospheric temperature inferred from spectra at maximum light ("shallow-silicon supernovae"). If the early light curve differences were driven entirely by interaction with a companion and viewing angle, the correlation with SNe Ia photospheric properties at maximum light is puzzling. When reaching maximum light, the ejecta has expanded by a factor of nearly 5000 in volume, is a factor of ∼50 brighter, and is now powered by radioactive decay rather than potentially from shock cooling. Any influence from a possible companion is likely shrouded at this stage in the SN Ia's evolution.

In addition to early-time light curves, nebular spectroscopy of SNe Ia provides the unique opportunity to place external constraints on the progenitor system. When the companion is struck by the ejecta, mass is liberated from the donor star (Wheeler et al. 1975). Initially shrouded by the ejecta, this unbound material is obscured until the SN Ia reaches the nebular phase (i.e., becomes optically thin). By placing limits on the non-detection of expected spectral features, statistical limits can be placed on the maximum amount of stripped/ablated material that could go undetected in the observed spectrum. By comparing the derived limits on unbound companion material to dedicated SN-companion interaction simulations in the literature (e.g., Marietta et al. 2000; Pan et al. 2012; Boehner et al. 2017) we can constrain the progenitor system of these SNe Ia. This analysis has been applied to a few dozen SNe Ia in the literature (Mattila et al. 2005; Leonard 2007; Lundqvist et al. 2013, 2015; Shappee et al. 2013, 2018; Maguire et al. 2016; Graham et al. 2017; Holmbo et al. 2018; Sand et al. 2018), with no significant detections of unbound companion material.

Most previous studies on the amount of unbound material in SNe Ia used the parameterized 1D simulations of Mattila et al. (2005), which calculated the expected emission from stripped material at 350 days after SN Ia peak brightness. To convert flux/equivalent width upper limits to unbound mass limits, linear scalings were employed (e.g., Leonard 2007). Recently, Botyánszki et al. (2018) utilized multidimensional radiative transfer codes to calculate the expected emission from 0.25 $M_{\odot}$ of unbound material. These results differed from those of Mattila et al. (2005) on two accounts: the amount of clumping in the stripped material, which resulted in higher emitted luminosities, and the scaling between stripped mass and emitted luminosity being closer to exponential than linear. More stringent mass limits can be placed on non-detections of H and He in nebular spectra of SNe Ia with these updated models. Additionally, Botyánszki et al. (2018) found that He I lines should also be present from H-rich unbound material, assuming that the stripped material has non-zero metallicity. Thus, He I emission can also be used to place constraints on both H-rich and He-rich donor stars.

ASASSN-18bt (SN 2018oh) was discovered by the All-Sky Automated Survey for SuperNovae (ASAS-SN; Shappee et al. 2014) on 2018 February 4.41 in the *K2* Campaign 16 field (Brown et al. 2018; Shappee et al. 2019). Because ASASSN-18bt was in the K2 field of view at the time of explosion, the rise is extremely well characterized, especially because this is the brightest SN Ia observed by Kepler thus far (Shappee et al. 2019), peaking at $B_{\rm max} \approx 14.3$ mag on MJD 58162.7 ± 0.3 (Li et al. 2019). ASASSN-18bt is located in UGC 04780 ($z = 0.010981$, Schneider et al. 1990) at a mere 52.7 ± 1.2 Mpc (Li et al. 2019). Additionally, Li et al. (2019) found no reddening from the host galaxy, so we adopt the Milky Way reddening $E(B-V) = 0.04$ mag (Schlafly & Finkbeiner 2011).

The mechanism driving the bump and blue excess in the early light curve of ASASSN-18bt is being debated. Shappee et al. (2019) compared the rising light curve of ASASSN-18bt to various theoretical models including ^{56}Ni mixing in the ejecta (Piro & Nakar 2013), interaction with a RLOF companion (Kasen 2010), possible interaction with a circumstellar wind (Piro & Morozova 2016), and synthetic light curves of double-detonation models (Noebauer et al. 2017). Based on the shape of the rise, Shappee et al. (2019) concluded that ^{56}Ni mixing models can span the observed behavior and interaction with a companion is disfavored due to the rapid rise present in models with a large enough signature. However, Dimitriadis et al. (2019a) analyzed a similar set of data and drew a contradictory conclusion, using the observed blue color of ASASSN-18bt during the bump as evidence against a DD system. This discrepancy warrants additional constraints on the progenitor system of ASASSN-18bt.

In this Letter, we present a nebular-phase Keck I/Low Resolution Imager and Spectrograph (LRIS) spectrum of ASASSN-18bt and place strong limits on the presence of any stripped companion material. In Section 2, we present our photometric and spectral data acquisition and reduction. In Section 3, we outline the our methodology in searching for emission signatures of a SD progenitor system. Finally, in Section 4, we apply these methods to our nebular spectrum of ASASSN-18bt, finding no evidence for stripped/ablated companion material and conclude a likely DD progenitor for ASASSN-18bt.

2. Nebular Spectra and Photometry

We obtained nebular spectroscopy of ASASSN-18bt on 2018-11-08 (MJD 58430.65, 268 days after peak *B*-band brightness) with the LRIS (Oke et al. 1995) on the Keck I telescope using the polarimeter that simultaneously measures the orthogonally polarized components (Goodrich et al. 1995).[4] Utilizing the 1.″0 slit, the reduced spectrum covers roughly 3000–10000 Å at a nominal resolution of ∼7 Å across the entire spectral range. The individual 2D spectra are reduced with `Lpipe`,[5] implementing typical spectral reduction tasks such as bias subtraction, flat-field correction, wavelength calibration using arc lamp exposures, and flux calibration using spectrophotometric standard stars. The extracted, 1D spectra are finally combined to produce a composite spectrum. By combining all the individual polarized spectra we create a "total intensity" (i.e., unpolarized) spectrum with an effective exposure time of 4800 s, which is shown in the top panel of Figure 4.

Spectrophotometric standard stars are good for relative flux calibration, however, slit losses, weather conditions, and instrumental effects can cause the resulting spectrum to deviate by a factor of a few from absolute flux calibration. As the analysis in Section 4 depends explicitly on the flux calibration

[4] The polarimeter module in LRIS was in place for other targets observed in the same night, but cannot be removed for individual targets.
[5] http://www.astro.caltech.edu/~dperley/programs/lpipe.html

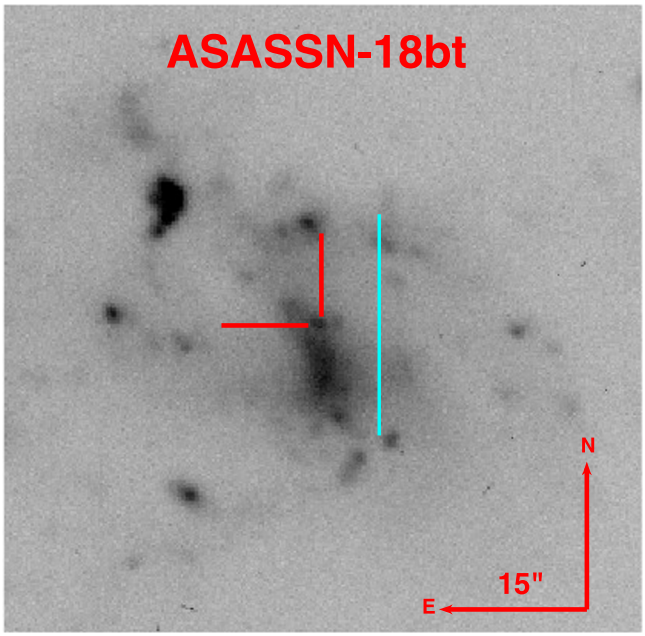

Figure 1. 1800 s OSMOS/MDM *r*-band image used for flux-calibrating the nebular spectrum. The location of ASASSN-18bt is indicated by the red ticks. The cyan line indicates the length and orientation of the 25″ long × 1″ wide LRIS slit used in the spectroscopic observations. The slit location is shifted horizontally for visual clarity.

of the observed spectrum, we need to place our spectrum on an absolute flux scale. First we perform aperture photometry on a 1800 s *r*-band image acquired on UT 2018-11-03 with the Ohio State MultiObject Spectrograph (OSMOS; Martini et al. 2011) on the MDM Observatory Hiltner 2.4 m telescope and is provided in Figure 1. Aperture photometry of ASASSN-18bt is conducted using the IRAF *apphot* package and calibrated to the ATLAS (Tonry et al. 2018a) All-Sky Stellar Reference Catalog (Tonry et al. 2018b). We measure an *r*-band magnitude of $r = 21.42 \pm 0.13$ mag, and changing the aperture and sky annulus radii did not substantially affect the resulting magnitude. To place the observed spectrum on an absolute flux scale, we calculate synthetic photometry from the nebular spectrum using Equation (7) from Fukugita et al. (1996) then scale the spectrum until the synthetic *r*-band magnitude equals the measured value. We estimate the final flux calibration of the nebular spectrum is good to the precision of the measured *r*-band magnitude (∼15%).

3. The Search for Unbound Companion Material

When a SN Ia explodes in the SD scenario, the SN Ia ejecta strikes the companion and removes material from the nearby donor star. Hydrodynamic simulations agree remarkably well on the amount and velocity distribution of unbound material from the RLOF donor star. For MS, SG, RG, and He-star companions we expected ∼0.2, ∼0.15, ∼0.5, and ∼0.03 $M_\odot$ to be removed from the donor star at velocities ∼750, ∼750, ∼600, and ∼1000 km s^{-1}, respectively. (Marietta et al. 2000; Liu et al. 2012, 2013; Pan et al. 2012; Boehner et al. 2017)

To search for emission from unbound companion material, we follow the methodology of Leonard (2007) with minor modifications. We fit the continuum with a second-order Savitzky–Golay polynomial (Press et al. 1992) using a smoothing width of 3000 km s^{-1}, which is wider than expected host galaxy lines and narrower than the intrinsic SN Ia ejecta emission lines. To prevent biasing our derived continuum, we fit the continuum omitting the spectral regions around each expected companion signature. We implement 3σ-clipping in our continuum fitting procedure to prevent instrumental artifacts, host galaxy lines, or telluric features from affecting the measured continuum.

After fitting the continuum, we subtract it from the observed spectrum and inspect the residuals for emission signatures indicative of material stripped/ablated from a RLOF companion. We inspect the same lines as those predicted by Botyánszki et al. (2018) for both H-rich and He-rich companions, including the Balmer series (Hα, Hβ, Hγ), and optical He I lines at 5876 and 6678 Å. We detect no emission lines with the velocity width expected for stripped material (∼1 000 km s^{-1}).

We then compute 5σ upper limits on the equivalent widths (EWs) of these lines using Equation (4) from Leonard & Filippenko (2001):

$$W(5\sigma) = 5\Delta I\sqrt{W_{\rm line}\Delta X} \quad (1)$$

where $W(5\sigma)$ is the 5σ upper limit on the EW of an undetected spectral feature, ΔI is the rms around a normalized continuum, $W_{\rm line}$ is the width of the spectral feature in Å, and ΔX is the bin size of the spectrum. Finally, we translate the EW upper limits into limits on unbound material assuming a distance of 49 Mpc and using the multidimensional radiative transfer calculations of Botyánszki et al. (2018) and the decay rate derived by M. A. Tucker et al. (2019, in preparation).

When placing limits on the presence of unbound companion material from the spectrum, underlying host-galaxy emission lines can contaminate the region of interest. Fortuitously, the SN ejecta ($v \sim 5000$ km s^{-1}), stripped/ablated companion material ($v \sim 1000$ km s^{-1}), and host-galaxy emission lines ($v \lesssim 100$ km s^{-1}) all have significantly different velocities (and therefore line widths). Thus, we are able to disentangle host galaxy and SN Ia ejecta emission from our derived $W(5\sigma)$, although the instrumental resolution of ∼300 km s^{-1} places a strict lower limit on any observed velocity profiles. While the host galaxy lines and possible telluric features will be narrower than our continuum smoothing, they will still affect our computed EW limits.

Host galaxy lines, including the Balmer series, S II, O III, N II, and Si II, are present in the reduced spectrum of ASASSN-18bt. We show a reduced 2D spectrum around Hα in Figure 2, which shows apparent narrow, host galaxy Hα emission extended along the spatial axis. While the velocity of this material ($\lesssim$300 km s^{-1}) is too low to originate from a stripped companion, it may indicate ASASSN-18bt stems from a young progenitor system. Further studies of the environment surrounding ASASSN-18bt, similar to Lyman et al. (2018), are warranted.

To mitigate contamination from the host galaxy, we mask out regions contaminated by host galaxy lines, telluric effects, and instrumental signatures in the reduced spectrum (gray regions in Figure 4). We implement a correction term to Equation (1) to account for these masked regions.

$$f = \sum_n G(p_i) \Big/ \sum_{i=1}^{N} G(p_i) \quad (2)$$

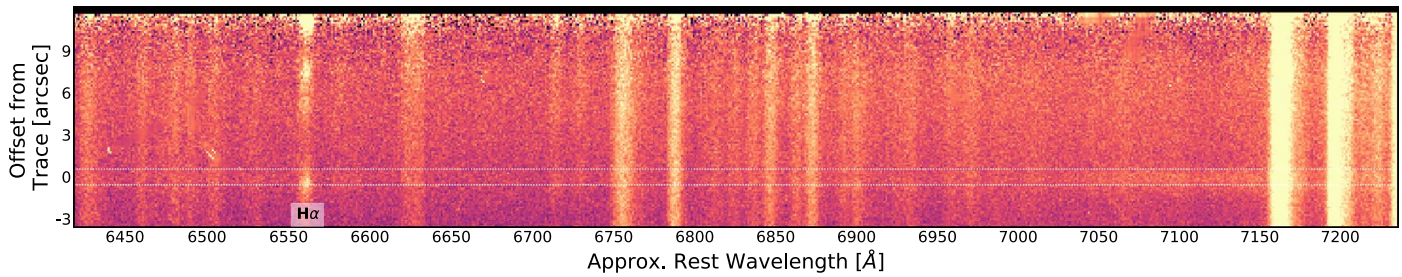

Figure 2. Slice of a reduced 2D spectrum of ASASSN-18bt. The extraction region of ASASSN-18bt is indicated by the faint horizontal white dotted lines. Extended Hα emission is present in the 2D spectrum, indicating the narrow Hα emission in Figure 4 originates from the host galaxy.

Table 1
Upper Limits on Undetected Spectral Features Expected from Unbound Companion Material

Line	$W_{\rm line}$ [Å]	$W(5\sigma)$ [Å]	Flux Limit [10^{-16} erg cm^{-2} s^{-1}]	Luminosity Limit [10^{37} erg s^{-1}]	H-rich Mass Limit [$M_\odot$]	He-rich Mass Limit [$M_\odot$]
Hα	21.9	0.169	1.50	4.32	0.006	…
Hβ	16.1	0.202	1.84	5.29	0.011	…
Hγ	14.5	0.225	2.05	5.88	>1	…
He I-a	19.6	0.095	0.85	2.44	0.005	0.020
He I-b	22.3	0.071	0.62	1.79	0.007	0.017

Note. He I-a and He I-b correspond to He Iλ5876 and He Iλ6678, respectively.

where p is the set of pixels in the spectral region, $G(p)$ is the Gaussian function computed at pixels p, N is the complete set of pixels, and n is the *unmasked* subset of pixels used in the limit determination (i.e., $n \subset N$, and $n \equiv N$ when there are no masked pixels in a given spectral region). By definition, $f \in [0, 1] \; \forall \; p$ and $f < 1$ when any pixels within 2 × FWHM of line center are masked (i.e., when $n \neq N$). This accounts for not using all pixels in the spectral region, but weighting each pixel by the Gaussian flux at that pixel because pixels near line center contain more information than pixels on the outskirts of the line. Thus, our 5σ statistical limit on the non-detection of a given spectral line becomes

$$W(5\sigma) = 5\Delta I f^{-1}\sqrt{W_{\rm line}\,\Delta X} \tag{3}$$

using the same nomenclature as Equations (1) and (2). This modified form of Equation (1) retains the same basic formulation while incorporating the exclusion of contaminated pixels near the expected emission features. Any masked pixels result in $f < 1$, and therefore increase the resulting $W(5\sigma)$, ensuring our statistical limit is robust.

4. Results

We compute flux, luminosity, and unbound mass upper limits for each of Hα, Hβ, Hγ, He Iλ5876, and He Iλ6678 using Equation (3), which are shown in Figure 4 and presented in Table 1. The gray regions correspond to masked locations in the final spectrum, with prominent masked regions including host galaxy Hα, Hβ, Hγ, N II, and S II.

4.1. Mitigating Host Galaxy Contamination

The 1D extracted spectrum of ASASSN-18bt includes several regions contaminated by host galaxy emission lines, including Hα. Because ASASSN-18bt is a serious SD system candidate based on the bump and color in the early light curve, all avenues must be explored when considering if the observed Hα emission stems from the host or the SN Ia itself. We find the probability of the observed Hα emission stemming from a non-degenerate H-rich companion extremely unlikely for the following reasons.

1. There is extended Hα emission present in the 2D spectrum (Figure 2).
2. The host galaxy has observed Hα emission in archival Sloan Digital Sky Survey spectra (Aguado et al. 2019).
3. Narrow Hα emission is also seen in the pre-maximum spectra, and is attributed to the host galaxy (Li et al. 2019).
4. The spatial profiles of ASASSN-18bt in the 2D spectrum are inconsistent at 2.2σ in line center and 3.5σ in line width (Figure 3).
5. The derived velocity of the Hα emission line ($\approx$300 km s^{-1}, the spectral resolution) is several factors too low compared to all dedicated hydrodynamic simulations in the literature (Marietta et al. 2000; Liu et al. 2012; Pan et al. 2012; Boehner et al. 2017).
6. There are other host galaxy lines observed in the nebular spectrum, such as S II and O III, which have comparable velocity profiles as the observed Hα line and are not expected to be prominent emission lines from unbound material (e.g., Botyánszki et al. 2018).
7. If the observed Hα emission was truly from a stripped companion, viewing angle should shift the emission profile shape and center of Hα (Botyánszki et al. 2018) unless the explosion happened while the companion was directly perpendicular to our line of sight.
8. Any stripped companion material will consist of solar metallicity material, not just pure H. In addition to H emission, this material should exhibit He I emission (Botyánszki et al. 2018), for which we have strict constraints (Table 1).

When masking the host galaxy Balmer emission lines, we first fit the width of the observed Hα profile with a measured FWHM of 6.98 Å ($\approx$300 km s^{-1}), which is essentially the

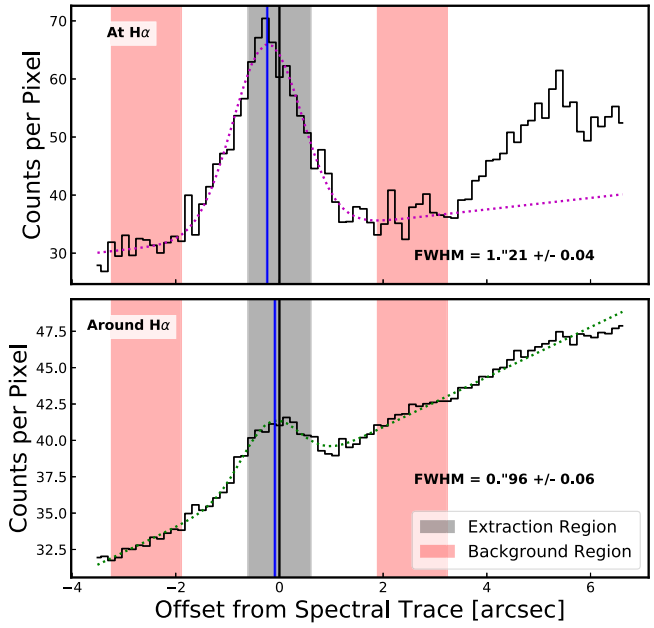

Figure 3. Spatial profiles of ASASSN-18bt at Hα (top) and the region surrounding (but excluding) Hα (bottom) in the combined 2D spectra. The vertical black line indicates the center of the spectral trace, whereas blue vertical lines represent the center of the fitted line profile (Gaussian + linear continuum) for each spatial slice. Only pixels within ±3″ of the spectral trace are included in the line profile fit. The fitted FWHM of each line profile is provided in the bottom right of each panel. The spatial profiles for ASASSN-18bt are discrepant at ∼3.5σ in width and ∼2.2σ in line center, indicating the spatial profile at Hα is influenced by host galaxy emission.

spectral resolution (i.e., the galaxy lines are unresolved). We mask (in velocity space) the same regions around Hβ and Hγ to ensure that we remove any possible host contamination, even if undetected, in our analysis of the unbound material emission lines. We also apply this method to the host galaxy N II and S II emission lines; however, these lines occur near the edges of their respective spectral regions of interest, and are therefore less critical to the final analysis. When computing the flux limit of a spectral region that includes masked portions of the spectrum, we use Equation (3) as described in Section 3.

4.2. Hydrogen-rich Companions

The limit on unbound H-rich material derived using Hα is slightly less stringent than the same limit derived from the He I-a line. However, the modeling for the Balmer series is more extensive than that of the helium emission, so we adopt this value for our limit. The strictest 5σ mass limit on stripped H-rich material, 0.006 $M_\odot$ from Hα, is far lower than the expected amount of unbound mass from simulations in the literature ($\gtrsim$0.15 $M_\odot$; Marietta et al. 2000; Pan et al. 2012; Boehner et al. 2017). Our statistical limit concretely rules out the possibility of a H-rich non-degenerate companion, including MS, SG, and RG models. Even considering the 3σ worst case scenario for distance (58 Mpc) and flux calibration ($r = 21.81$ mag), our limits on H-rich unbound material are an order of magnitude stronger than the expected stripped material.

4.3. Helium Star Companions

In addition to H-rich non-degenerate companions, helium star donors have also been proposed as possible progenitor systems for SNe Ia. Helium stars are typically the result of binary interaction, making them reasonable candidates for SN Ia progenitors. In the literature, there have been a few studies on possible effects of SN ejecta impacting a nearby RLOF He star. Pan et al. (2012) and Liu et al. (2013) performed hydrodynamic simulations modeling the interaction between the SN ejecta and the stellar surface, finding 0.023–0.057 $M_\odot$ of material is removed from the donor star by the explosion (He-r model from Pan et al. 2012 and W7_He01/2_r models from Liu et al. 2013).

Botyánszki et al. (2018) also performed non-local thermodynamic equilibrium spectral modeling to predict line luminosities from He-rich unbound material. However, Botyánszki et al. (2018) did not self-consistently implement the velocity and density distributions from helium star hydrodynamic simulations, but instead replaced the unbound mass from the MS model with pure helium. We inherently assume the same scaling between mass and luminosity for He-rich material as H-rich material, which is reasonable and likely more accurate than 1-to-1 scaling relations previously assumed in the literature. However, we conservatively view our He-rich mass limits as tentative, until more detailed theoretical studies are conducted.

Our results place strong statistical limits on the amount of He-rich unbound companion material, with 5σ upper limits of 0.020 $M_\odot$ and 0.017 $M_\odot$ for He Iλ5876 and He Iλ6678, respectively. These mass limits rule out even the least-stripped helium star models discussed above. Furthermore, even in the absence of our limit, we note that a helium star companion would be too small ($\lesssim$0.4 $R_\odot$, see Liu et al. 2013) to explain the large early-time blue excess observed in the K2 light curve of ASASSN-18bt.

5. Conclusion and Discussion

In this Letter, we present the first nebular spectral analysis of ASASSN-18bt, a SNe Ia observed by *K2* moments after explosion. Although pre-peak data for ASASSN-18bt is exquisite in terms of precision and temporal sampling, the interpretation is inconclusive. One of the most enigmatic features of ASASSN-18bt is the two-component rising light curve (Dimitriadis et al. 2019a; Shappee et al. 2019). Previously, similar features have been interpreted as potential ejecta-companion interaction (e.g., Hosseinzadeh et al. 2017). The Shappee et al. (2019) analysis of the rising *K2* light curve of ASASSN-18bt favors shallow ^{56}Ni models over companion interaction models, whereas the analysis conducted by Dimitriadis et al. (2019a) concludes a likely SD progenitor system as the origin of the bump and blue excess. This discrepancy warrants additional independent constraints on ASASSN-18bt's progenitor system.

With our nebular-phase Keck I/LRIS spectrum acquired 268 days after *B*-band maximum, we constrain the amount of H and He emission from possible unbound companion material. Using available models in the literature (Botyánszki et al. 2018), we convert our non-detection of H and He emission lines into upper limits on the amount of unbound mass. The resulting H and He mass limits rule out non-degenerate H-rich and (tentatively) He star companions (Figure 4, Table 1).

Because a SD progenitor system does not match the observed early- and nebular-phase constraints, we consider a DD system as the likely progenitor of ASASSN-18bt. However, there is still the question of what causes the initial rise in the early light curve. As discussed in Shappee et al. (2019), a small amount of ^{56}Ni in the outer layers of the ejecta

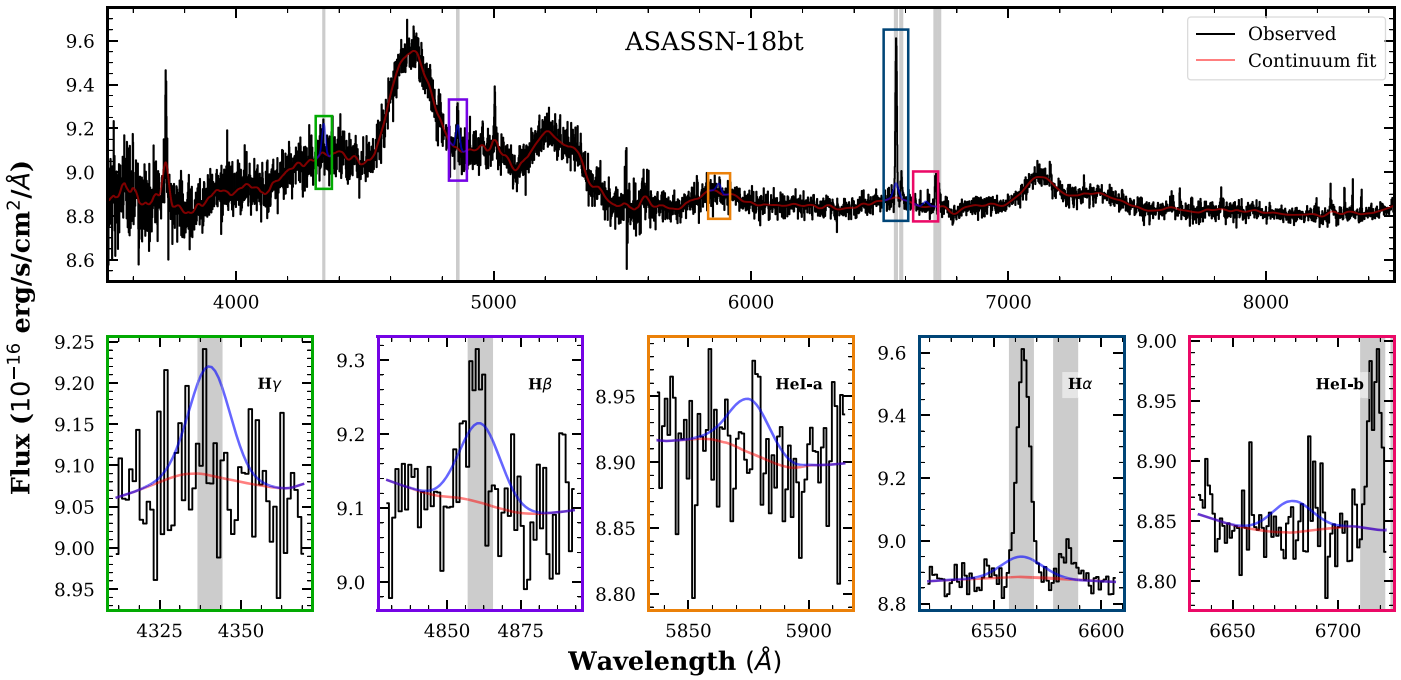

Figure 4. Flux-calibrated nebular spectrum of ASASSN-18bt from Keck I/LRIS. Insets: Zoomed in view of the region around each expected emission line, denoted in the top-right corner, showing the observed spectrum (black), our continuum fit (red), and the empirical flux limit (blue). Axis colors correspond to the boxed locations in the top panel. These flux limits rule out all H-rich RLOF non-degenerate companions and (tentatively) rule out He-rich donors as well (see Table 1). Gray regions mark masked pixels which are excluded from our continuum fit and the derived $W(5\sigma)$ (see Section 3).

may reproduce the observed early light curve component. Furthermore, there is possible direct evidence for shallow ^{56}Ni in the nearby SN 2014J; a SN Ia that also exhibited an early rise that cannot be explained by a single power law (Goobar et al. 2015; Siverd et al. 2015). Diehl et al. (2014) and Isern et al. (2016) claimed detections of the 158 keV ^{56}Ni gamma-ray decay lines in SN 2014J between 16 and 35 days after explosion, requiring $\sim$0.05 $M_\odot$ of shallow ^{56}Ni.

Early-time SNe Ia light curves have revealed unexpected diversity, giving us additional views into their progenitor systems. Yet, while rapid progress has been made, there are still large uncertainties in our understanding of these progenitors systems. This uncertainty highlights the continuing need for increased theoretical and observational work.

During the review process for this manuscript, Dimitriadis et al. (2019b) released a similar independent paper on nebular spectra of ASASSN-18bt. The findings of both studies are in agreement, each placing strict upper limits on the possibility of any unbound companion material.

We thank the referee for their useful comments and improvement of the manuscript. We thank Justin Rupert (MDM), Joshua Shields, and Krzysztof Stanek (Ohio State University) for acquiring the finding MDM *r*-band image. We thank Gagandeep Anand, Connor Auge, Aaron Do, Ryan Foley, Anna Payne, Jose Prieto, and Jennifer van Saders for useful discussions. M.A.T. acknowledges support from the United States Department of Energy through the Computational Sciences Graduate Fellowship (DOE CSGF).

ORCID iDs

M. A. Tucker https://orcid.org/0000-0002-2471-8442
B. J. Shappee https://orcid.org/0000-0003-4631-1149
J. P. Wisniewski https://orcid.org/0000-0001-9209-1808

References

Aguado, D. S., Ahumada, R., Almeida, A., et al. 2019, ApJS, 240, 23
Antognini, J. M., Shappee, B. J., Thompson, T. A., & Amaro-Seoane, P. 2014, MNRAS, 439, 1079
Boehner, P., Plewa, T., & Langer, N. 2017, MNRAS, 465, 2060
Botyánszki, J., Kasen, D., & Plewa, T. 2018, ApJL, 852, L6
Brown, J. S., Stanek, K. Z., Vallely, P., et al. 2018, ATel, 11253, 1
Cartier, R., Sullivan, M., Firth, R. E., et al. 2017, MNRAS, 464, 4476
Contreras, C., Philips, M. M., Burns, C. R., et al. 2018, ApJ, 859, 24
Diehl, R., Siegert, T., Hillebrandt, W., et al. 2014, Sci, 345, 1162
Dimitriadis, G., Foley, R. J., Rest, A., et al. 2019a, ApJL, 870, L1
Dimitriadis, G., Rohas-Bravo, C., Kilpatrick, C. D., et al. 2019b, ApJL, 870, L14
Dong, S., Katz, B., Kushnir, D., & Prieto, J. L. 2015, MNRAS, 454, L61
Fink, M., Röpke, F. K., Hillebrandt, W., et al. 2010, A&A, 514, A53
Fukugita, M., Ichikawa, T., Gunn, J. E., et al. 1996, AJ, 111, 1748
Goobar, A., Kromer, M., Siverd, R., et al. 2015, ApJ, 799, 106
Goodrich, R. W., Cohen, M. H., & Putney, A. 1995, PASP, 107, 179
Graham, M. L., Kumar, S., Hosseinzadeh, G., et al. 2017, MNRAS, 472, 3437
Holmbo, S., et al. 2018, arXiv:1809.01359
Hosseinzadeh, G., Sand, D. J., Valenti, S., et al. 2017, ApJL, 845, L11
Hoyle, F., & Fowler, W. A. 1960, ApJ, 132, 565
Iben, I., & Tutukov, A. V. 1984, ApJS, 54, 335
Isern, J., Jean, P., Bravo, E., et al. 2016, A&A, 588, A67
Jiang, J.-A., Doi, M., Maeda, K., et al. 2017, Natur, 550, 80
Kasen, D. 2010, ApJ, 708, 1025
Katz, B., et al. 2012, arXiv:1211.4584
Kromer, M., Sim, S. A., Fink, M., et al. 2010, ApJ, 719, 1067
Lanz, T., Telis, G. A., Audard, M., et al. 2005, ApJ, 619, 517
Leonard, D. C. 2007, ApJ, 670, 1275
Leonard, D. C., & Filippenko, A. V. 2001, PASP, 113, 920
Li, W., Wang, X., Vinkó, J., et al. 2019, ApJ, 870, 12
Liu, Z.-W., Pakmor, R., Seitenzahl, I. R., et al. 2013, ApJ, 774, 37
Liu, Z.-W., Telis, G. A., Audard, M., et al. 2012, A&A, 548, A2
Lundqvist, P., Mattila, S., Sollerman, J., et al. 2013, MNRAS, 435, 329
Lundqvist, P., Nyholm, A., Taddia, F., et al. 2015, A&A, 577, A39
Lyman, J. D., Taddia, F., Stritzinger, M. D., et al. 2018, MNRAS, 473, 1359
Maguire, K., Taubenberger, S., Sullivan, M., & Mazzali, P. A. 2016, MNRAS, 457, 3254
Maoz, D., Mannucci, F., & Nelemans, G. 2014, ARA&A, 52, 107
Marietta, E., Burrows, A., & Fryxell, B. 2000, ApJS, 128, 615

Martini, P., Stoll, R., Derwent, M. A., et al. 2011, PASP, 123, 187
Mattila, S., Lundqvist, P., Sollerman, J., et al. 2005, A&A, 443, 649
Miller, A. A., Cao, Y., Piro, A. L., et al. 2018, ApJ, 852, 100
Noebauer, U. M., Kromer, M., Taubenberger, S., et al. 2017, MNRAS, 472, 2787
Nugent, P. E., Sullivan, M., Cenko, S. B., et al. 2011, Natur, 480, 344
Oke, J. B., Cohen, J. G., Carr, M., et al. 1995, PASP, 107, 375
Pakmor, R., Kromer, M., Taubenberger, S., et al. 2012, ApJL, 747, L10
Pan, K.-C., Ricker, P. M., & Taam, R. E. 2012, ApJ, 750, 151
Pejcha, O., Antognini, J. M., Shappee, B. J., & Thompson, T. A. 2013, MNRAS, 435, 943
Piro, A. L., & Morozova, V. S. 2016, ApJ, 826, 96
Piro, A. L., & Nakar, E. 2013, ApJ, 769, 67
Press, W. H., et al. 1992, Numerical Recipes in FORTRAN. The Art of Scientific Computing (2nd ed.; Cambride: Cambridge Univ. Press)
Rebassa-Mansergas, A., Toonen, S., Korol, V., & Torres, S. 2019, MNRAS, 482, 3656
Sand, D. J., Graham, M. L., Botyánszki, J., et al. 2018, ApJ, 863, 24
Schlafly, E. F., & Finkbeiner, D. P. 2011, ApJ, 737, 103
Schneider, S. E., Thuan, T. X., Magri, C., & Wadiak, J. E. 1990, ApJS, 72, 245
Shappee, B. J., Holoien, T. W.-S., Drout, M. R., et al. 2019, ApJ, 870, 13
Shappee, B. J., Piro, A. L., Stanek, K. Z., et al. 2018, ApJ, 855, 6
Shappee, B. J., Prieto, J. L., Grupe, D., et al. 2013, ApJL, 762, L5
Shappee, B. J., Prieto, J. L., Grupe, D., et al. 2014, ApJ, 788, 48
Shappee, B. J., Stanek, K. Z., Kochanek, C. S., & Garnavich, P. M. 2017, ApJ, 841, 48
Shappee, B. J., & Thompson, T. A. 2013, ApJ, 766, 64
Shen, K. J., Boubert, D., Gänsicke, B. T., et al. 2018, arXiv:1804.11163
Siverd, R. J., Goobar, A., Stassun, K. G., & Pepper, J. 2015, ApJ, 799, 105
Stritzinger, M. D., Shappee, B. J., Piro, A. L., et al. 2018, ApJL, 864, L35
Thompson, T. A. 2011, ApJ, 741, 82
Tonry, J. L., Denneau, L., Flewelling, H., et al. 2018b, ApJ, 867, 105
Tonry, J. L., Denneau, L., Heinze, A. N., et al. 2018a, PASP, 130, 064505
Tutukov, A. V., & Yungelson, L. R. 1979, AcA, 29, 665
Webbink, R. F. 1984, ApJ, 277, 355
Wheeler, J. C., Lecar, M., & McKee, C. F. 1975, ApJ, 200, 145
Woods, T. E., Ghavamian, P., Badenes, C., & Gilfanov, M. 2018, ApJ, 863, 120
Zheng, W., Silverman, J. M., Filippenko, A. V., et al. 2013, ApJL, 778, L15